45TH TURBOMACHINERY & 32ND PUMP SYMPOSIA
HOUSTON, TEXAS | SEPTEMBER 12 – 15, 2016
GEORGE R. BROWN CONVENTION CENTER

AERO-DAMPING MEASUREMENTS AND COMPUTATION IN A FULL-SCALE MULTISTAGE CENTRIFUGAL COMPRESSOR

Dr. Lorenzo Toni
Lead Engineer
GE Oil & Gas – Nuovo Pignone
Florence, Italy

Dr. François Moyroud
Engineering Technical Leader
GE Oil & Gas – Thermodyn
Le Creusot, France

Dr. Dante Tommaso Rubino
Engineering Manager
GE Oil & Gas – Nuovo Pignone
Florence, Italy

Dr. Giuseppe Gatta
Senior Engineer
GE Oil & Gas – Nuovo Pignone
Florence, Italy

Dr. Alberto Guglielmo
Lead Engineer
GE Oil & Gas – Nuovo Pignone
Florence, Italy

Dr. Kishore Ramakrishnan
Mechanical Engineer
Aerodynamics and Acoustics Lab, GE Global Research
Niskayuna NY, USA

Lorenzo Toni is a Lead Engineer in the Radial Turbomachinery Aerodynamic Design Team within the Advanced Technology Organization of GE Oil & Gas. His responsibilities include the centrifugal compressors aerodynamic design, unsteady aerodynamics and aeromechanic modelling and analysis. Lorenzo joined GE in 2009 as a Test and Data Analysis Engineer and then moved to his present position. He received an M.S. degree in Mechanical Engineering from the Florence University in 2005 and earned a PhD in Energetics from the same University in 2009, with a doctoral research in the area of heat transfer and advanced cooling systems design for combustor liners, turbine endwalls and blades. He is the author or co-author of several technical papers in the field of turbomachinery.

Giuseppe Gatta is a Senior Engineer of the Conceptual Mechanical Design Team within the Turbomachinery Solutions Organization. He has been with GE Oil & Gas since 2010. His main areas of expertise are aeromechanics, structural dynamics and acoustics as well as static analysis and fatigue calculation. He has been dedicated to improving the aeromechanical design of axial compressor blades and centrifugal compressor impellers, holding technical leadership both for numerical and test activities. He capitalizes on Six Sigma concepts, methodologies and tools to improve product quality and competitiveness. Since his studies he has been pursuing increase of predictive capabilities and numerical-test correlation. He received his M.S. degree in Aerospace Engineering from University of Naples.

Alberto Guglielmo is a Design Engineer for New Product Introduction group at GE Oil & Gas. He received his M.Sc. in Mechanical Engineering from the University of Pisa in 2004 and a PhD degree in Mechanical Engineering from the University of Pisa in 2008. He joined GE Oil & Gas in the 2008 working for Requisition Team for centrifugal compressor and in 2011 he moved to New Product Introduction (NPI) team. He has been involved into both analytical and experimental structural dynamic and machine design.

François Moyroud is an Engineering Technical Leader at Thermodyn, entity of GE Oil & Gas, in France. He joined the New Product Introduction group as Senior Engineer in 2008. His responsibilities cover the aerodynamic performance of low to medium pressure centrifugal compressors, including integrated electric machines, as well as the experimental and numerical validation of the aeromechanical design of new stages. He has been working with Turbomachinery Aeromechanics for 20 years. He holds a PhD from the National Institute of Applied Sciences of Lyon and from the Royal Institute of Technology of Stockholm. He started his career as Research Assistant, and developed numerical methods to predict military and civil aero engine fan blade flutter. He then joined the Aerospace industry in the UK in 2000 where he acted as aeromechanics specialist on military engine development programs until 2007. He is a member of the ASME.

Tommaso Rubino is currently the Manager of the Radial Turbomachinery Aerodynamic Design and Performance within the Advanced Technology Division of GE Oil & Gas Company, in Florence, Italy. His responsibilities include the aerodynamic design and the performance predictability of the GE Oil & Gas turbocompressors and turboexpanders product lines. Dr. Rubino joined GE in 2006 as Design Engineer in Centrifugal Compressor NPI team, then rolling in the Aero team upon creation of the Advanced Technology Organization, where he has been responsible of the aerodynamic design of new stage families for Centrifugal Compressors. Mr. Rubino received an M.S. degree in Mechanical Engineering in 2002 and a Ph.D. degree in Mechanical Engineering in 2006 from Politecnico of Bari, and he graduated with honors in the Diploma Course program at the von Karman Institute in 2002.

Kishore Ramakrishnan is a member of the Aerodynamics and Acoustics Lab at GE Global Research in Niskayuna, New York. He joined GE in 2006 after obtaining a Masters and PhD in Mechanical Engineering from Purdue University in West Lafayette, Indiana. He develops fan and turbomachinery noise reduction technologies and improved prediction methods with primary application to aircraft engines and gas turbines. He also led development of high fidelity analysis methods as well as reduced order models for centrifugal compressor acoustic-structure interaction. He is a senior member of the AIAA and has served as session organizer and technical paper reviewer for the ASME on many occasions.

ABSTRACT

Great interest is being paid by Oil & Gas industry to the design of high speed and high pressure ratio centrifugal compressors. Static and dynamic stresses are becoming higher and, under critical conditions, aerodynamic forcing may lead to impeller high cycle fatigue failures. Thorough aeromechanics knowledge is hence necessary for the advanced design of centrifugal compressors, to ensure reliability and life-time. Open impellers, which are commonly used for high speed applications, may be prone to relatively high vibration levels, due to aerodynamic excitations present in the flow field. Indeed, resonant crossings with forcing functions are in some cases unavoidable in variable speed machines since a wide speed range results in a wide frequency range of rotor-stator interactions, as well as flow-field circumferential distortions, occurring at multiples of the impeller excitations.

Impeller forcing amplitudes and aeromechanical damping both contribute to vibratory response levels and must be properly predicted. This paper is focused on the aerodynamic damping prediction. A comprehensive study was undertaken to develop and validate aerodynamic damping prediction capability for open impellers for the operating conditions and mode shapes of interest. An extensive experimental campaign was conducted on a full scale multistage compressor equipped with transonic unshrouded impellers instrumented with strain gauges connected to a telemetry system. The strain gauge data are compared to the CFD (Computational Fluid Dynamics) predicted damping for blade and disk modes and show good agreement. The present paper describes the challenges related to aerodynamic damping prediction in a real machine environment taking into account complex flow features, for example flow distortions, off-design conditions and different pressure levels.

The level of agreement between test data and CFD predictions achieved in this work represents a significant step forward towards building and validating a fully physics based predictive capability for open impeller forced response. In fact, such validated aerodynamic damping prediction capability is required for aeromechanic risk mitigation and accurate impeller high cycle fatigue analysis in early stages of the design process.

INTRODUCTION

Over the last few decades the maximum rotational speeds and mass flow rates of centrifugal compressors have been progressively increased resulting in higher mean stresses on impellers. To achieve higher rotational speeds (peripheral speeds) the impeller shroud has been removed resulting in lighter open impellers which can be used on the first stages (with larger external diameters) and mixed with closed or shrouded impellers in hybrid configurations. The OEM describes this as the High Pressure Ratio Compressor (HPRC) technology, which is based on an architecture that combines unshrouded and shrouded impellers on a single high speed shaft to achieve pressure ratios and efficiency levels higher than other available technologies. HPRC provides a compact and efficient compressor configuration with a significant reduction of compression train footprint and fewer stages. The more compact the configuration is, the stronger the blade row interactions are, with consequently higher unsteady fluid-structure interactions.

On this kind of technology platform, the relatively thin blades of open impellers are more vulnerable to alternating stresses and could suffer from high cycle fatigue failures. Full aeromechanical validation is hence considered mandatory for the complete qualification of these stages.

An appropriate requirement for open blading can be found within API 617 (2002) under the Axial Compressor section. According to this standard, "the blade natural frequencies shall not coincide with any source of excitation from 10% below minimum allowable speed up to 10% above maximum continuous speed (MCS). If this is not feasible, blading shall be designed with stress levels low enough to allow unrestricted operation, at any specified operating speed for the minimum service life established for the machine". This shall be verified by plotting Goodman diagrams or their equivalent.

Fundamentally, two main quantities are needed when one tries to trace an analytical Goodman plot by estimating the response level for a specific structural mode shape: damping and modal work. The physical stress (σ_{phys}) can be determined as a scaling of the modal stress (σ_{modal} available via a finite element analysis) according to Eq. (1), see also Appendix:

$$\sigma_{phys} = \frac{F_{modal} \cdot Q}{\omega^2} \cdot k \cdot \sigma_{modal} \tag{1}$$

$$Q = \frac{1}{2\zeta}; \quad F_{modal} = \left| \Phi_i^t F \right| \tag{2}$$

Where F_{modal} (usually calculated from an ad-hoc developed tool) is the modal force computed by integrating the dot product of the unsteady pressure over the impeller main flow and secondary flow path surfaces with the specific structural mode shape; f is the impeller mode natural frequency (predicted with a finite element analysis); Q is the damping factor and k is a factor introduced to take into account a blade-to-blade or sector-to-sector variability or other uncertainties in the prediction. The Q-factor includes all the types of damping even if, for an impeller of centrifugal compressors, the aerodynamic damping is predominant since friction damping is not present and material damping is relatively small. The importance of the aerodynamic damping in the forced response evaluation is discussed by Srinivasan (1981) for axial machines, and Dickmann et al. (2006) as well as in Kammerer and Abhari (2008) for radial machines. This is highlighted in Figure 1: the Goodman diagram reported on the left for a generic mode shape is obtained using only material damping, whereas on the right all stresses scale sensibly down once aerodynamic damping is included.
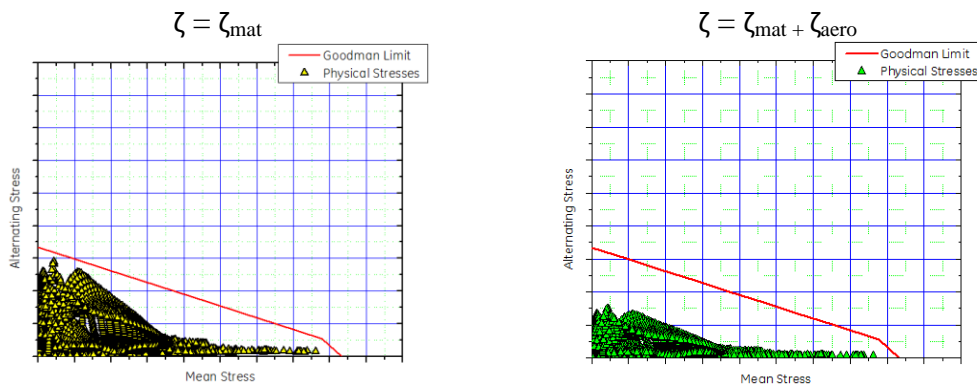

Figure 1 – Example of Aero-Damping Effect on Goodman Diagram

The process of extracting aeromechanical damping from strain gauge data is somewhat well established and discussed, for example, by Kammerer and Abhari (2008), Dickmann et al. (2009), and Bidaut and Baumann (2012). In the absence of test data and without damping prediction capability, engineers have to estimate the aerodynamic damping based on experience. However this is a challenging exercise since the damping varies not only with the flow conditions (gas density, inlet pressure, design versus choke flow etc.) but also with the impeller mode shape (blade bending mode versus disk mode, nodal diameter pattern etc.). So clearly design engineers need a physics-based aerodynamic damping prediction capability. It is evident from the open literature that aerodynamic damping calculations are routinely used on axial machines to assess the risk of blade flutter instabilities. On the other hand, the authors have found very few publications reporting aerodynamic damping predictions on centrifugal impellers, including for example the work of Dickmann et al. (2009) and Krishnababu et al. (2010).

In this paper, we will present the result of a continued effort to develop and validate a robust process to accurately compute aerodynamic damping for radial machines. A validated predictive capability is essential to quickly screen impeller designs, reducing product development costs and improving product quality for better competitive positioning. All numerical results presented in this paper have been correlated to a series of experimental measurements collected during HPRC prototype aeromechanical test runs. The CFD validation performed both on impeller disk and blade modes will show that aeromechanical damping predictions compare well with the machine test data.

NUMERICAL METHODOLOGY

The CFD analysis was performed using a proprietary Reynolds Averaged Navier-Stokes flow solver. The solver is a three-dimensional cell-centered finite volume multi-block, multi-grid, structured non-linear and time harmonic (frequency domain) unsteady solver for turbomachinery blade rows, as reported in Holmes et al. (1997). The numerical method is described in detail in Clancy et al. (2014) and in Ren et al. (2016) and is only summarized here for brevity. A choice of common two-equation turbulence models is available to compute the steady flow. This numerical solver is routinely used in performance predictions as part of the design process. More details may be found in Guidotti et al. (2011), Satish et al. (2013) and Guidotti et al. (2014).

A time-linearized Navier–Stokes method was applied to predict the aerodynamic damping. Time harmonic results were obtained by linearizing the underlying steady flow numerical algorithm. Solutions were obtained via explicit time marching, with multigrid, on multiblock grids. The calculations were performed with the assumption that the phenomenon of interest – for example flow separation or a shock – already has to be present in the steady flow field and the motion is a small disturbance about a computed steady solution.

In cyclic symmetry, for a tuned system, all blades vibrate with the same amplitude and frequency, but phase lagged in time; such lag is commonly known as the Inter Blade Phase Angle (IBPA) or more generally the periodic sector phase angle, see also Crawley (1985), defined in Eq. (3):

$$IBPA = 2\pi \frac{ND}{N} \tag{3}$$

where ND refers to the nodal diameter of the impeller mode shape under analysis and N is the number of periodic sectors on the impeller. For an impeller with main blades and splitter blades as it is the case in this study, the periodic sector consists of one main blade and one splitter blade.

A Giles nonreflecting boundary condition is employed at the inlet and exit boundaries of the impeller to minimize numerical reflections caused by acoustic waves emanating from the blade row wall vibration. Phase lagged boundary conditions are applied to the periodic sector boundaries to enforce an inter-blade phase angle consistent with the nodal diameter of the vibration mode of interest. Note that with an inter-blade phase angle boundary condition it is sufficient to model a single blade passage of the impeller to simulate the dynamic behavior and unsteady flow response of the full wheel.

The aerodynamic work is defined as the work removed by the fluid from the vibrating impeller over a cycle of vibration, Figure 2. If the work is positive, the fluid is removing energy from the impeller motion, and is considered stabilizing (same nomenclature used in the frame work of axial machine blade flutter instabilities). Conversely, if the work is negative, the fluid is adding energy to the motion and is considered destabilizing. Knowing the frequency and modal mass associated with the vibration mode, the aerodynamic work may be converted into an equivalent aerodynamic damping.

The prediction process has been applied to model tests of different impellers with good success. The chart shown in Figure 3 includes open and closed impellers, blade and disk modes, as well as high and low speed stages. Material damping has been subtracted from the test data and results are scaled to 1 bar inlet pressure to allow a consistent comparison across a variety of test conditions. In general, prediction quality is very good, providing confidence in applying the methodology to the more complex situation described in this paper.
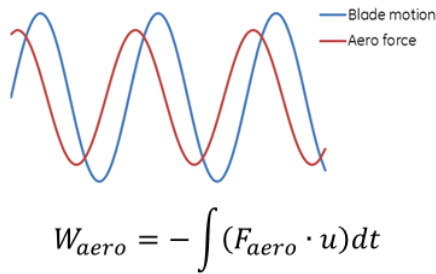
$$W_{aero} = -\int (F_{aero} \cdot u)dt$$

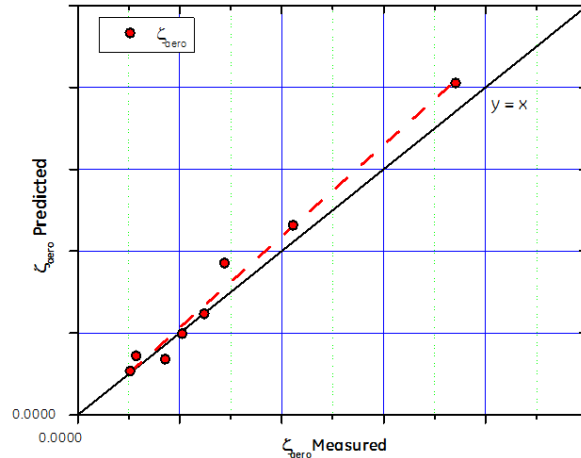**Figure 2 – Schematic Illustration of Aerodynamic Work on a Vibrating Airfoil**

Figure 3 – Validation of Prediction Process against Model Test Data

EXPERIMENTAL CAMPAIGN

Test Bench and Instrumentation

The HPRC prototype test was performed on a permanent test bench which consists of three independent gas loops, an auxiliary system (lube oil, DGS and cooling) and an electric motor driver; see also Falomi et al. (2016). Maximum allowable power absorption for the testing cell is about 10 MW. The machine was equipped with standard instrumentation to measure and control the thermo-dynamic performance and special instrumentation to validate compressor behavior under both steady state and transient conditions. In particular, instrumentation for validation of mechanical and thermo-mechanical behavior comprises:

- Strain gauges on first section open impellers for aeromechanic validation
- Strain gauges and thermocouples on rotor tie-rod
- Thermocouples on diaphragms and casing
- Temperature measurements on Dry Gas Seal
- Load cells on thrust bearings
- Accelerometers on compressor external casing

The strain gauges used for the aeromechanic validation were positioned on the main walls of open impeller at main blades, splitter blades and disk; as shown in Figure 4.

Strain gauge signals are transmitted by a telemetry system that consists of a rotating unit and a stationary unit. The rotating unit is equipped with a miniaturized sensor signal amplifier, A/D conversion module and a radio transmitter, whereas the stationary unit includes an antenna and D/A conversion module.

Strain gauge position and orientation are optimized by avoiding sensor placement in areas of high stress gradient. This arrangement allows good observability of the selected set of mode shapes as well as providing robustness of the measurements The quality of strain gauge positioning is expressed in term of mode sensitivity ratio and strain gradient. The mode sensitivity ratio is defined as the ratio of the strain measured at strain gauge position versus the maximum stress for an arbitrary scale factor of the mode shape. The strain gradient is defined as the ratio between the gradient of the strain in the direction of measurement versus the average strain. The best practice for strain gauge positioning requires a minimum value for sensitivity and a low local stress gradient in order to minimize the measurement error due to sensor position installation tolerances.
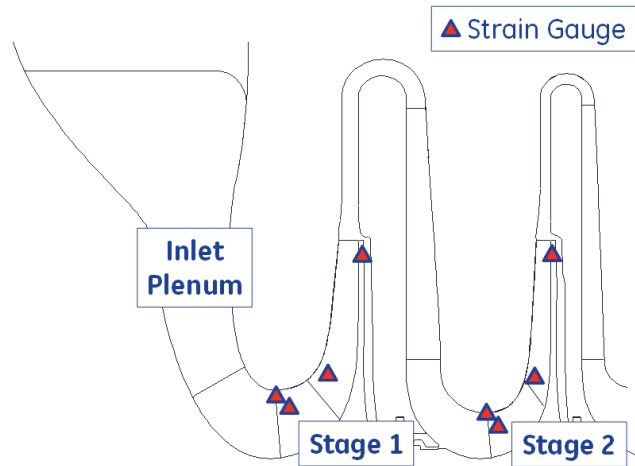
Figure 4 – Schematic of the Strain Gauges (Triangles) on the Open Impellers of Full Scale Compressor

Two impellers were tested. A set of four gauge positions was chosen for each impeller to clearly detect the impeller mode shapes predicted inside the compressor operating range. The four gauges on each impeller were located as follows: two strain gauges on a main blade, one on a splitter blade and one on the disk. Each position is replicated over multiple sectors on the impeller to guarantee redundancy and estimate the sector-to-sector variability. Figure 5 shows the strain gauge positions on the first open impeller of the HPRC prototype.

Figure 5 – Impeller with Strain Gauges

Test Methodology and Post-Processing

During the aeromechanic test, the compressor speed is continuously ramped up from minimum operating speed (MOS) to maximum continuous speed (MCS) in order to cover the entire design space of the impellers. During a speed ramp, the impeller is subjected to a multi tone sine sweep excitation generated by the aerodynamic drivers existing in the machine.

Impeller vibrations are continuously measured and recorded with a sampling rate of 51 kHz. The signals in time domain are divided into a sequence of windows and converted into the frequency domain. The spectrum sequence is reported in cascade in a waterfall diagram. The vibration amplitudes at different engine orders are extracted and the experimental Campbell diagrams for all strain gauges are monitored. The acceleration ratio of the machine during each speed ramp is small enough to ensure a pseudo stationary signal with limited frequency variation inside each window and at the same time with enough frequency in the reconstructed Campbell diagram. Figure 6 shows the waterfall and the Campbell diagram for a typical speed ramp up. The excitation of structural mode is highlighted by a frequency modulation of the synchronous forced response in the Campbell diagram and by the presence of random response not tracked with the speed in the waterfall diagram.
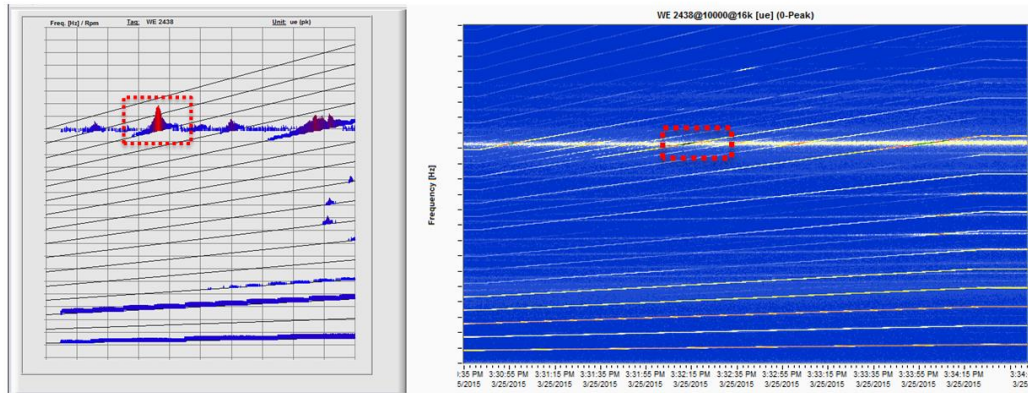
Figure 6 – Waterfall Diagram and Experimental Campbell Diagram

The amplitude response of each strain gauge is fitted with a single degree of freedom (SDOF) numerical model and the modal damping (aero + mechanical) is obtained. Figure 7 shows an example of curve fitting (red curve) applied to experimental data (yellow dots) for a specific resonant crossing.
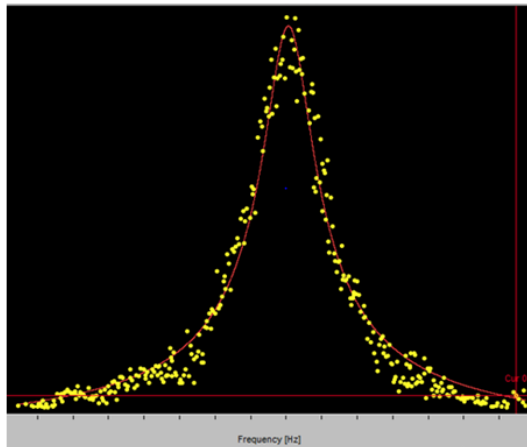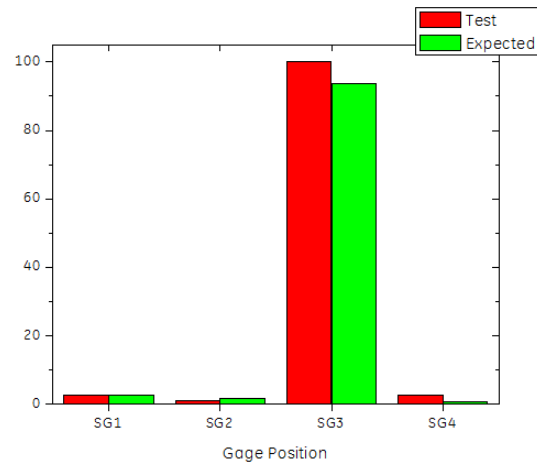

Figure 7 – SDOF Response Fitting at Strain Gauge

Figure 8 – Matching Between Numerical and Experimental Mode Shape

A simplified modal assurance criterion (MAC) is used to identify the excited mode such that the contribution of the modes out of resonance is assumed negligible (SDOF approach). The amplitude ratio between different strain gauges calculated with finite element (FE) model is compared with the measured value and the match is evaluated. Figure 8 shows a comparison of numerical and experimental strain ratios for a pure bending mode of the blade.

By means of the transfer functions derived from a finite element model, the strain measured at the SG location is related to the one at the impeller critical point on the Goodman diagram. 100% scope limit is obtained when the maximum allowable strain at the critical point in the Goodman diagram is reached: see Figure 9. When the measured strain gauge ratios and FE modal shapes are consistent, strain amplitudes at resonance can be used to scale the Goodman diagram and to perform a fatigue assessment of the impeller.
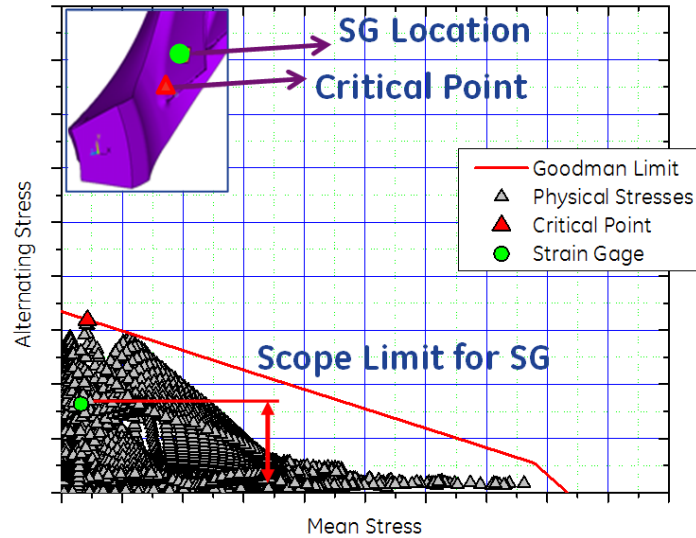
Figure 9 – Scope Limit Definition at Strain Gauge Location

RESULTS AND DISCUSSION

Excitation Source and Resonant Crossings

Results will focus on the first stage open impeller of the multistage compressor, see again Figure 4. Flow distortions from the inlet plenum were initially considered to be a source of only low order excitations: however as shown in Figure 10, the inlet plenum flow field contains a wide range of circumferential harmonics. Although many harmonics have low magnitudes, they may interact with the downstream impeller generating unsteady loading variations.

The results of the finite element modal analysis of the impeller are used to identify the potential resonant crossings between the aforementioned aerodynamic drivers and the structural mode shapes. FE computations have been performed under the assumption of cyclic symmetry, including a pre-stressed static analysis so as to take into account centrifugal loads. The impeller mode shapes are grouped in terms of nodal diameters (ND), or harmonic index (HI). The difference between ND and HI is well explained in Bertini et al. (2014). A nodal diameter is an ideal line of zero modal displacement whereas the harmonic index represents the same information about mode shapes complexity looking only at relative blade displacements. Therefore a continuous structure like the hub supporting the blades can exhibit a large number of nodal diameters but the blades itself can have a smaller number of phase changes and the same shape appears with a lower complexity. The impeller modes are represented against frequency on a SAFE diagram shown in Figure 11, see also Singh et al. (1988). The tested impeller was designed with 22 blades (11 main blades + 11 splitter blades). Since excitation patterns may be expressed in terms of nodal diameters or circumferential order, the SAFE diagram is a smart and useful way to identify the resonance condition both in terms of frequency coincidence and mode shape correspondence (nodal diameter and engine order) between the structural mode and the unsteady aerodynamic driver.
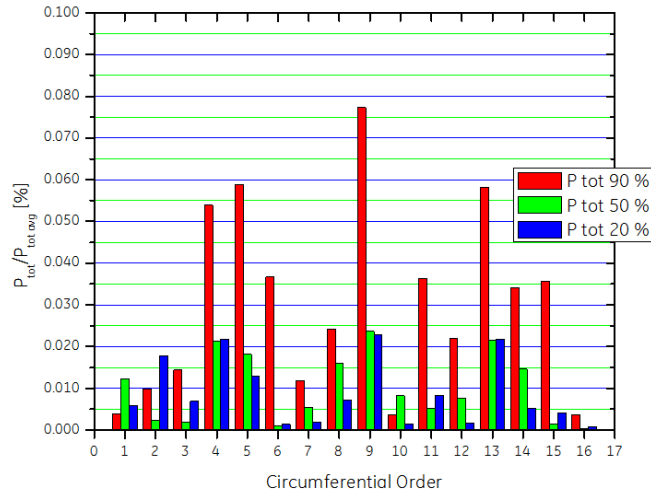
Figure 10 – Inlet Plenum Harmonics at Different Span Positions from Steady State CFD

Potential resonant crossings were identified between disk modes having 6ND to 9ND and their corresponding engine orders frequencies (harmonics of shaft rotation frequency, indicated in the text as *n/Rev*) and between blade first flexural modes and higher order drivers (from 11*/Rev* to 16*/Rev*), refer again to Figure 11 where mode shapes are shown.

Experimental campaign has been a fundamental step not only for the assessment of the different resonant crossings, in terms of response levels and aerodynamic damping, but also to verify the accuracy in predicting the interactions and to confirm the absence of unexpected interferences. We will here focus on the resonant crossings which showed high response levels: two modes with high hub disk participation, having 7 and 8 nodal diameters respectively, and a blade first flexural mode (MB 1F), excited by the 14*/Rev*. These cases were numerically analyzed using the approach discussed previously.
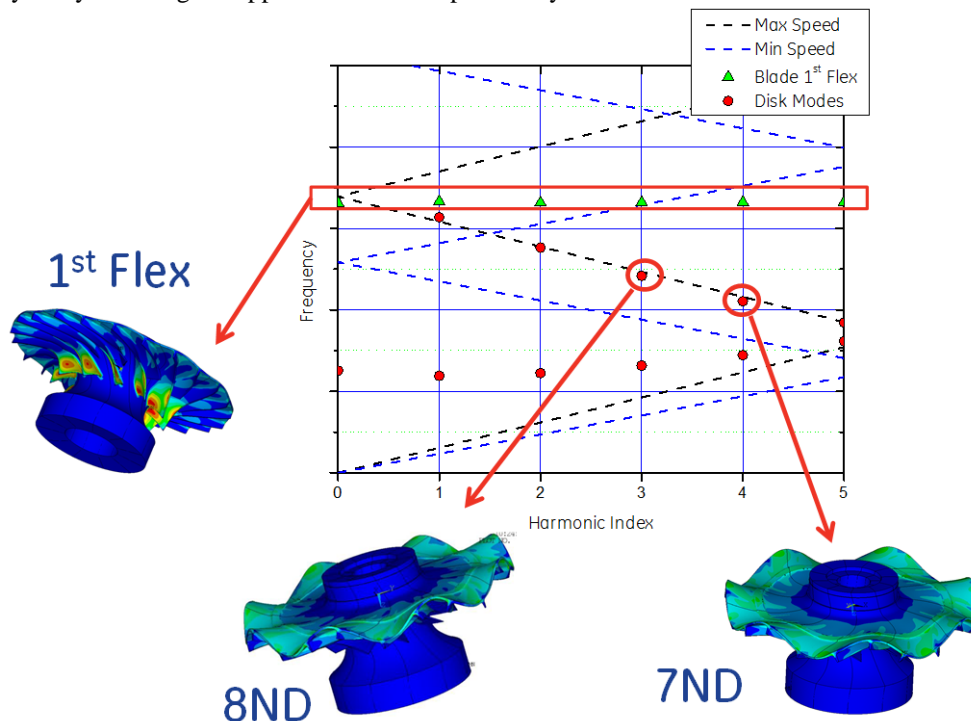

Figure 11 – Interference Diagram

Material Damping Evaluation

It is well known that the overall aeromechanical damping is the sum of material, mechanical and aerodynamic damping: the second contribution is commonly neglected for impellers, since no energy dissipation through component friction is present; hence the critical damping ratio may be expressed as the sum of the remaining two, as in Eq. (4):

$$\zeta(P) = \zeta_{mat} + \zeta_{aero}(P) \tag{4}$$

where P represents dependency with a gas static pressure on the impeller wetted surfaces.

Overall damping, is then the sum of the pressure dependent aerodynamic damping and the pressure independent (though mode dependent) material damping, as also proposed by Kammerer and Abhari (2009) and by Zemp and Abhari (2012). For the purposes of the present work, and also for sake of generalization, we prefer to re-write Eq. (4) in terms of density (ρ), Eq. (5): the effect of different gas compositions and operating conditions is then taken into account.

$$\zeta(\rho) = \zeta_{mat} + \zeta_{aero}(\rho) \tag{5}$$

Using the same approach of the aforementioned authors and of Gilbert et al (2012), material damping is evaluated for the different mode shapes by extrapolating the experimental data to zero density (in-vacuum modal damping). The obtained values have then been added to the numerically predicted aerodynamic damping to obtain the aeromechanical damping.

As already mentioned, the aeromechanical campaign was conducted in order to perform an extensive validation of the impeller mechanical design criteria: hence design and off-design operating conditions, both inside and outside machine normal operating range, have been explored. Listed below are the flow parameters varied during the testing phase:

- Flow rate variations from stage choke to left limit
- Gas composition
- Inlet gas density

Disk Modes Damping

Figure 12 represents the measured damping values, in black symbols, as a function of average density, for the impeller disk trailing edge mode with 7 nodal diameters. Damping values shown in the aforementioned figure, as well as hereafter, have been normalized by the average damping. The spread in the experimental data is mainly due to gauge-to-gauge variability, gas compositions for a given gas density and different operating conditions (i.e. flow coefficient ranging from choke to left limit) considered. The whole data set has been analyzed, following the approach described in the previous section, to evaluate the material damping value as per Equation 5. As a first outcome, the analysis of Figure 12 shows a linear increase of aeromechanic damping with the increasing density.

A subset of the experimental data, represented on the same plot in red, corresponds, in terms of molecular weight, to the CFD simulation results which are shown as green circles: this subset helps in quickly identifying which test data and predictions are directly comparable to each other. Predictions are all within the range of test data: moreover, besides correctly getting the trend with density, the CFD computation correctly captures the effect of flow coefficient at a constant density (see the three points at density of approximately 6.7).

Interesting observations may be drawn from the analysis of Figure 13. The aerodynamic work obtained from the numerical computations is shown here for the different vibrating impeller surfaces: disk hub wall on the cavity side (left), blade pressure side wall (center) and blade suction side wall (right). Bearing in mind that negative aerodynamic work means positive damping (i.e. gas taking energy out of motion), we may conclude that while the impeller blades provide a neutral contribution (due to the opposing effect of suction and pressure sides) the hub disk wall generates a large amount of positive damping.
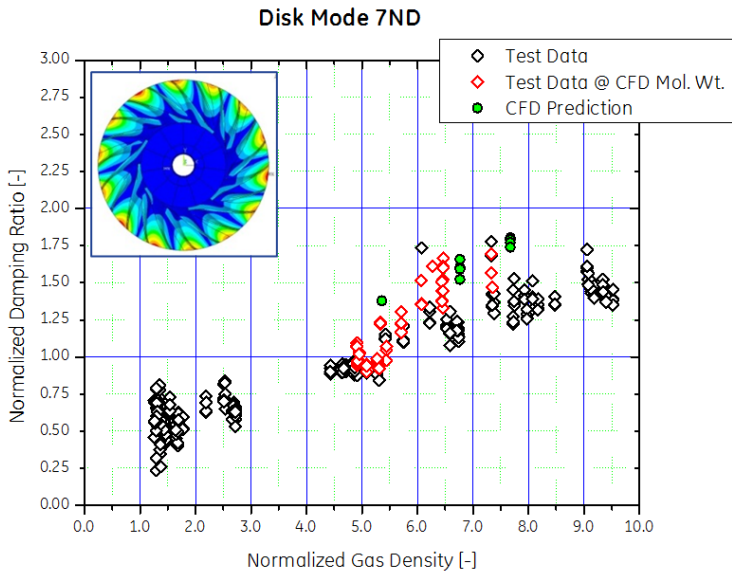
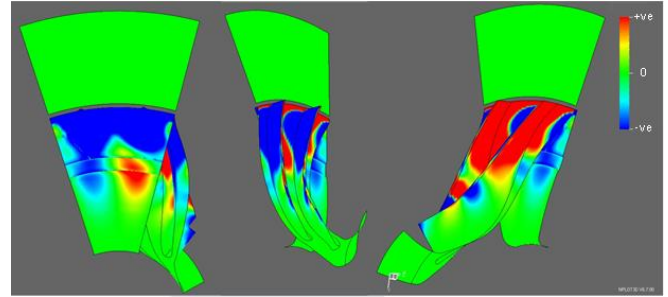Figure 12 – Normalized Damping, 7 ND Mode

Figure 13 – Aerodynamic Work for 7 ND Mode

We now analyze the results obtained for the disk mode with 8 nodal diameters, see the mode shapes shown in Figure 11. Critical damping ratio, represented against gas density is shown in Figure 14, while Figure 15 depicts the aerodynamic work on the impeller; very similar conclusions may be drawn for this resonant crossing as well. Again, an almost linear trend of aeromechanic damping with gas density is seen and the comparison between numerical predictions and test data is very encouraging. As far as the aerodynamic work for this vibration mode is concerned, Figure 15, the balancing effect of negative and positive work on blades pressure and suction sides, respectively, leads, on the whole, to a null effect. On the contrary, the hub disk side wall generates negative aerodynamic work, which means positive damping. This points to the importance of modeling the cavities to accurately capture the aerodynamic damping.
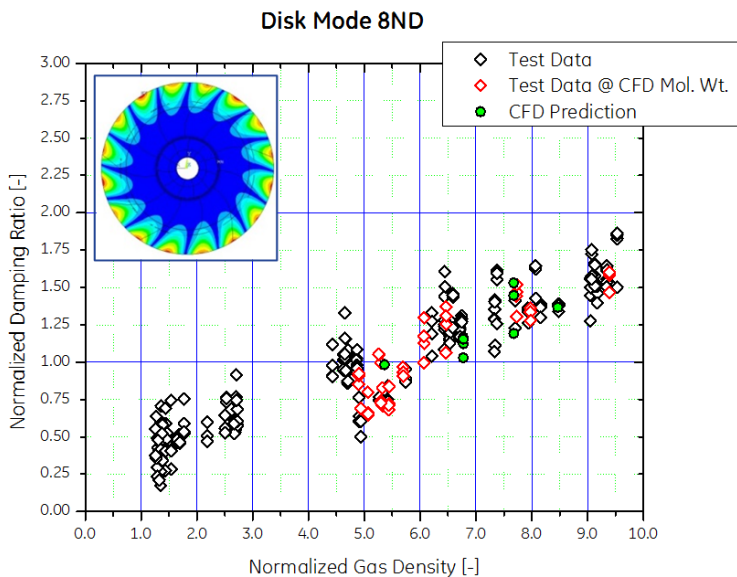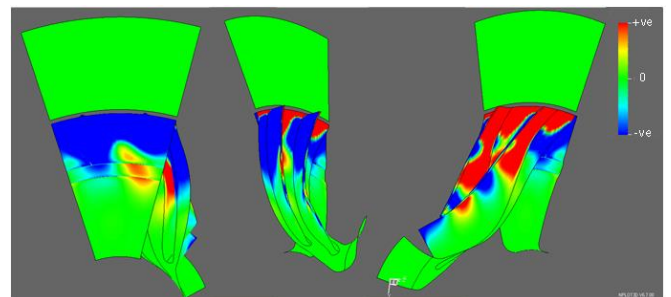

Figure 14 – Normalized Damping, 8 ND Mode

Figure 15 – Aerodynamic Work for 8 ND Mode

In order to evaluate the effect of flow coefficient on aeromechanic damping, a regression fit based on inlet flow coefficient (φ) and inlet momentum (ρv) has been performed on the test data. Then, for a given thermodynamic condition used for the CFD computations of disk modes with 7 and 8 nodal diameters, the regression has been used to represent the experimentally measured damping. Figure 16 shows the comparison: even though slight differences in absolute values are observable, the CFD predictions capture the decrease in damping observed experimentally as we move from design point to choke flow.
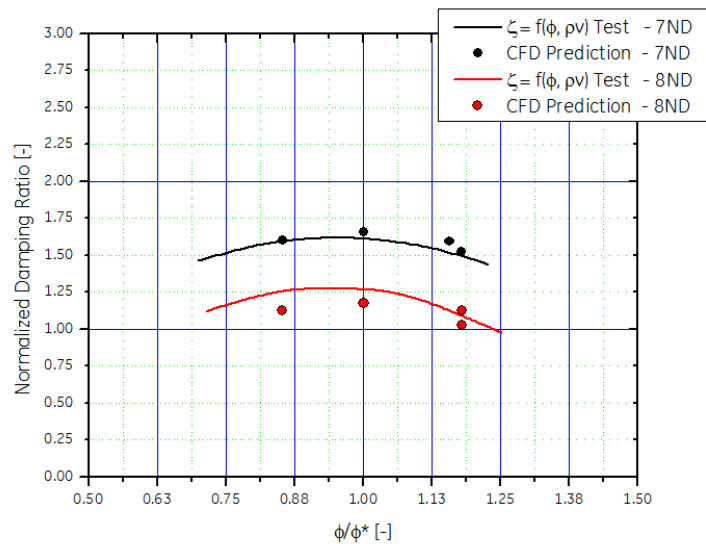

Figure 16 – Normalized Critical Damping Ratio vs. Flow Coefficient

Main Blade First Flexural Mode Damping

Concerning the interactions between main blade first flexural mode shapes and the drivers corresponding to engine orders from 11 to 16/*Rev*, we will focus on the resonant crossing with the 14/*Rev* since this is the one which showed the highest measured response level on the strain gauges. Hence it can be expected to provide the most accurate estimate of modal damping. Figure 17 shows measured and expected damping values: a linear behavior with density is evident and once more predictions are well aligned with test data. The analysis of aerodynamic work contours, Figure 18, shows a different scenario with respect to disk modes: indeed the hub surface gives a neutral contribution to damping, whereas the leading edge region of main blade suction side shows a wide area of negative work and hence positive damping.

The plot shown in Figure 19 summarizes all the conclusions drawn from the aerodynamic work analysis both for disk modes and for blade first flex mode. The relative magnitude of damping over the different impeller surfaces highlights in a more quantitative way the "cancellation effect" of pressure and suction side damping for disk modes (red and green bars) and the absolute need of including the side cavity in CFD model to completely describe the phenomenon. For main blade first flex modes, it is clear that only the main blade contributes to modal damping. Thus, details of the cavity model are not critical for such modes.
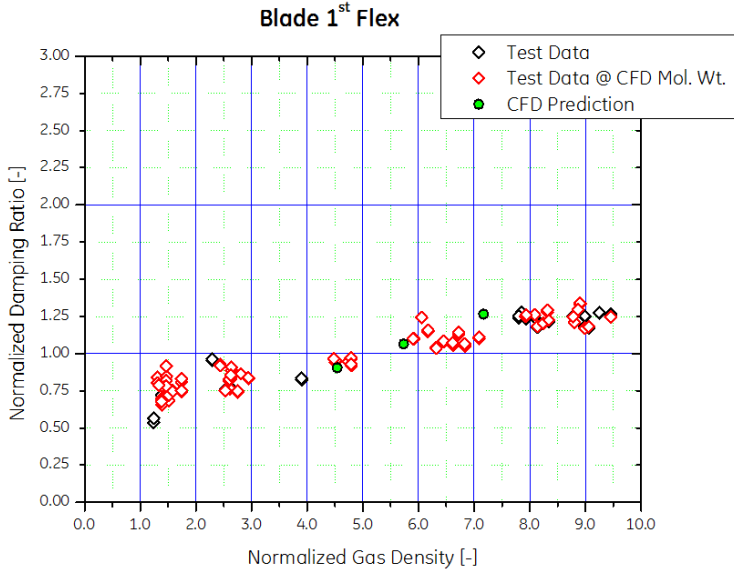
Figure 17 – Normalized Damping, MB 1st Flex HI3 Mode
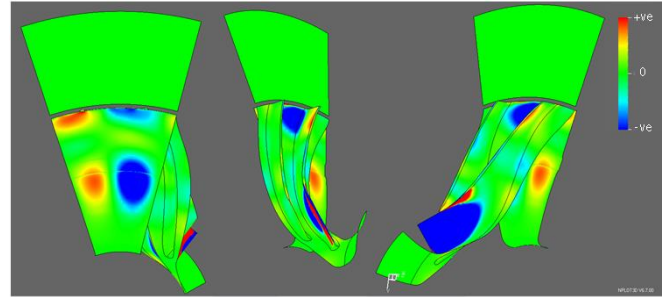
Figure 18 – Aerodynamic Work for MB 1st Flex HI3 Mode

Nomenclature for Figure 19	
MB	Main Blade
SB	Splitter Blade
PS	Pressure Side
SS	Suction Side
TE	Trailing Edge
Hub	Disk Hub Wall in Main Flow
Cavity	Disk Hub Wall in Cavity Side
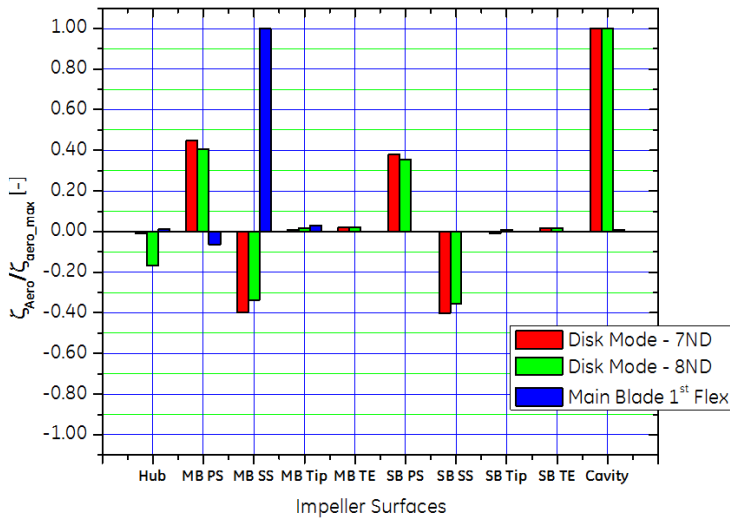
Figure 19 – Aerodynamic Damping Distribution Over Impeller Surfaces

CONCLUSIONS

This paper showed the results of an extensive aeromechanical test campaign conducted on a three-section full-scale centrifugal compressor, whose first section was equipped with two open impellers instrumented with several strain gauges.

Test results, in terms of aeromechanical damping of the first stage impeller were compared to CFD predictions obtained through a proprietary flow solver, using a computational process previously validated on several single stage model tests.

Three different mode shapes were analyzed: two disk modes (with 7 and 8 nodal diameters respectively) and a main blade first flexural mode. A very good agreement between test data and predictions was found for the different operating conditions (mainly pressure level and flow coefficient). The computational approach was demonstrated to be robust and reliable, capable of correctly predicting not only aerodynamic damping trends but also absolute values, even in somewhat off-design conditions. The importance of modeling detailed geometrical features (e.g. hub cavity in this case) was highlighted.

In summary, full aeromechanical validation is becoming fundamental in the design process of centrifugal compressors due to higher rotor speeds and pressure ratios. Accurate aerodynamic damping estimation under realistic flow conditions as shown in this paper is a crucial enabler in building a predictive capability to assess and mitigate aeromechanical risk.

NOMENCLATURE

D	= Impeller External Diameter	[m]
f	= Frequency	[Hz]
F	= Aerodynamic Motion Independent Force	[N]
F_{aero}	= Aerodynamic Motion Dependent Force	[N]
F_{modal}	= Aerodynamic Modal Force (Motion Independent)	depends on mode shape normalization
k	= Blade to Blade variability Factor	[-]
N	= Number of Sectors	[-]
P	= Pressure	[Pa]
Q	= Damping Amplification Factor	[-]
Q_{vol}	= Volumetric Flow Rate	[m^3/s]
u	= Peripheral Speed	[m/s]

Greeks

φ	= Flow Coefficient $\dfrac{4Q_{vol}}{\pi D^2 u}$	[-]
φ*	= Design Flow Coefficient	[-]
Φ	= Mode Shape	depends on normalization
ρ	= Density	[kg/m^3]
σ	= Stress	[MPa]
ζ	= Overall Critical Damping Ratio	[-]
$ζ_{aero}$	= Aerodynamic Critical Damping Ratio	[-]
$ζ_{mat}$	= Material Critical Damping Ratio	[-]
ω	= Frequency	[rad/s]

Acronyms

CFD	= Computational Fluid Dynamics
FE	= Finite Elements
IBPA	= Inter Blade Phase Angle
HI	= Harmonic Index
HPRC	= High Pressure Ratio Compressor
MAC	= Modal Assurance Criterion
MCS	= Maximum Continuous Speed

MOS   = Minimum Operating Speed
Mol. Wt.   = Molecular Weight
ND   = Nodal Diameter
OEM   = Original Equipment Manufacturer
SDOF   = Single Degree of Freedom
SG   = Strain Gauge

APPENDIX

  The dynamic equilibrium equations Eq. (6) can be resolved in modal domain using the properties of mode shapes. The mode shapes Φ represent a base of vectorial space and each physical quantity, i.e. the vector X of displacement, can be expressed as a linear combination of n vectors Φ_i that are function of space, and n $y_i(t)$ functions of time Eq. (7).

$$M\ddot{X}(t) + C\dot{X}(t) + KX(t) = F(t) \tag{6}$$

$$X(t) = \sum_{i=1}^{n} \Phi_i \cdot y_i(t) \tag{7}$$

The orthogonal properties of mode shapes Φ allows the uncoupling of dynamic equations and the matrix system (6) is converted in a series on n independent systems, Eq. (8), in the variable y(t) that represents the response of each mode shape for the given excitation.

$$\ddot{y}_i(t) + 2\zeta_i\omega_i(t)\dot{y}_i(t) + \omega_i^2 y_i(t) = \Phi_i^t F(t) \quad i = 1\dots n \tag{8}$$

  Eq. (8) can be converted in frequency domain, Eq. (9) and, under the assumption of single-degree-of-freedom (SDOF) that allows excluding the contribution of out of resonance modes, the response amplitude at resonance peak ω_i of i-eth shape is given by Eq. (10).

$$y_i(\omega) = \frac{\Phi_i^t F}{\omega_i^2 - \omega^2 + 2i\zeta_i\omega_i\omega} \tag{9}$$

$$|y_i(\omega_i)| = \frac{|\Phi_i^t F|}{2\zeta_i\omega_i^2} \tag{10}$$

REFERENCES

API 617, 2002, Axial and Centrifugal Compressors and Expander-compressors for Petroleum, Chemical and Gas Service Industry, API Standard 617, 7th Edition.

Bertini, L., Neri, P., Santus, C., Guglielmo, A., and Mariotti, G., Analytical Investigation of the Safe Diagram for Bladed Wheels – Numerical and Experimental Validation, Journal of Sound and Vibration 333 (19) (2014) 4771–4788, DOI: 10.1016/j.jsv.2014.04.061.

Bidaut, Y., Baumann, U., Identification of Eigenmodes and determination of the Dynamical Behavior of Open Impellers, ASME Paper GT2012-68182.

Clancy, C., Moyroud, F., and Ramakrishnan, K., 2014, Effect of Cavities on Impeller Aeromechanical Forcing in a Low Pressure Ratio Centrifugal Compressor Stage, ASME Paper GT2014-27304.

Crawley, E. F., 1985, Aeroelastic Formulations for Turbomachines and Propellers, AGARD Manual on Aeroelasticity in Axial-Flow Turbomachines, NATO.

Dickmann, H.P., et al., 2006, Unsteady Flow in a Turbocharger Centrifugal Compressor: Three-Dimensional Computation Fluid Dynamics Simulation and Numerical and Experimental Analysis of Impeller Blade Vibration, Journal of Turbomachinery, 128, 455-465

Dickmann, H.P., et al., 2009, Unsteady Flow in a Turbocharger Centrifugal Compressor: 3D-CFD Simulation, Impeller Blade Vibration and Vaned Diffuser-Volute Interaction, ASME Paper GT2009-59046.

Falomi, S., Iurisci, G., Fattori, S., Grimaldi, A., Aringhieri, C., Sassanelli, G. And Iannuzzi, G., 2016, Full Scale Validation of a High Pressure Ratio Centrifugal Compressor, 45th Turbomachinery Symposium.

Gibert, C., Blanc, L., Almeida, P., Leblanc X., Ousty, J.-P., Thouverez, F. and Lainé, J.-P., 2012, Modal Tests and Analysis of a Radial Impeller at Rest: Influence of Surrounding Air on Damping, ASME Paper GT2012-69577.

Guidotti, E., Tapinassi, L., Toni, L., Bianchi, L., Gaetani, P., and Persico, G., 2011, Experimental and Numerical Analysis of the Flow Field in the Impeller of a Centrifugal Compressor Stage at Design Point, ASME Paper GT2011-45036.

Guidotti, E., Toni, L., Rubino, D. T., Tapinassi, L., Naldi, G., Satish, K., and Prasad, S., 2014, Influence of Cavity Flows Modeling on Centrifugal Compressor Stages Performance Prediction Across Different Flow Coefficient Impellers, ASME Paper GT2014-25830.

Holmes, D.G., Mitchell, B.E., and Lorence, C.B., 1997, Three Dimensional Linearized Navier-Stokes Calculation for Flutter and Forced Response, ISUAAT Symposium, Sweden.

Kammerer, A., and Abhari, R. S., 2009, Experimental Study on Impeller Blade Vibration During Resonance Part 2: Blade Damping, Journal of Engineering for Gas Turbines and Power, *131 (2)*, pp. 022509-9.

Krishnababu, S.K., Imregun, M., Green, J.S., Hoyniak, D., 2010, Aerodynamics and Aeroelasticity of Impeller Vaned Interactions in a High Pressure Ratio Centrifugal Compressor, ASME Paper GT2010-22595.

Ren et al., 2016, Investigations of Flutter and Aero Damping of a Turbine Blade Part 2: Numerical Simulations, ASME Paper GT2016-57935.

Satish, K., Guidotti, E., Rubino, D. T., Tapinassi, L., and Prasad, S., 2013, Accuracy of Centrifugal Compressor Stages Performance Prediction by Means of High Fidelity CFD and Validation Using Advanced Aerodynamic Probe, ASME Paper GT2013-95618.

Singh, M. P., Vargo, J. J., Schiffer, D. M. and Dello, J. D., 1988, Safe Diagram – A Design Reliability Tool for Turbine Blading, Proceedings of the 17th Turbomachinery Symposium, Turbomachinery Laboratory, Texas A & M University, College Station, Texas, pp. 93-101.

Srivastava, R., Lentz, J., Liu, J.S., Panovsky, J., 2007, Computation of Unsteady Flow Field and Blade Response due to Impeller-Diffuser Interaction, ASME Paper GT2007-28235.

Srinivasan, A. V., Cutts, D. G., and Sridhar, S., 1981, NASA, Technical Report No. NASA-CR-165406.

Zemp, A., and Abhari, R. S., 2012, Vaned Diffuser Induced Impeller Blade Vibrations in a High-Speed Centrifugal Compressor, Journal of Turbomachinery, *135 (2)*, pp. 0210115-9.

ACKNOWLEDGEMENTS

Copyright© 2016 by Turbomachinery Laboratory, Texas A&M Engineering Experiment Station